Supplementary Information for "DC-operated Josephson junction arrays as a cryogenic on-chip microwave measurement platform"

Senne Vervoort[1*], Lukas Nulens[1], Davi A. D. Chaves[1], Heleen Dausy[1], Stijn Reniers[1], Mohamed Abouelela[1], Ivo P. C. Cools[2], Alejandro V. Silhanek[3], Margriet J. Van Bael[1], Bart Raes[4], Joris Van de Vondel[1*]

[1]Quantum Solid-State Physics, Department of Physics and Astronomy, KU Leuven, Celestijnenlaan 200D, Leuven, B-3001, Belgium.
[2]Department of Microtechnology and Nanoscience, Chalmers University of Technology, Gothenburg, SE-412 96, Sweden.
[3]Experimental Physics of Nanostructured Materials, Q-MAT, Université de Liège, Allée du 6 Août 19, Sart Tilman, B-4000, Belgium.
[4]IMEC, Kapeldreef 75, Leuven, B-3001, Belgium.

*Corresponding author(s). E-mail(s): senne.vervoort@kuleuven.be; joris.vandevondel@kuleuven.be;
Contributing authors: lukas.nulens@kuleuven.be; daviadchaves@gmail.com; heleen.dausy@gmail.com; stijn.reniers@kuleuven.be; M.M.M.Abouelela@tudelft.nl; cools@chalmers.se; asilhanek@uliege.be; margriet.vanbael@kuleuven.be; bart.raes@imec.be;

1 Supplementary note 1: Impact of non-linear VI characteristics on radio-frequency emission

In this section, we discuss the effect of the non-linear regime in the VI curves on the measured spectrum. Apart from the occurrence of expected higher harmonics, we also notice that the FWHM increases in the non-linear regime of the VI-curve. The radiation is highly sensitive to voltage differences between the junctions, which is

most pronounced in the non-linear regime. This becomes clear in Fig. 1a which shows the VI characteristics of MoGe-bot at frustrations $\tilde{f} = 0$ and 1. The horizontal lines indicate voltages corresponding to 3.6 GHz and 4.4 GHz. At these voltages, spectra are measured and shown in Fig. 1b. The dashed lines are spectra measured at $\tilde{f} = 0$, i.e. when the VI is non-linear. The full lines are spectra measured at $\tilde{f} = 1$, where the VI is more linear. Comparing the spectra in these two situations, the emission is much broader in the non-linear regime at $\tilde{f} = 0$. Furthermore, at 3.6 GHz in the most non-linear part, the emitted power is reduced as well, compared to the spectrum in the more linear range of the VI at $\tilde{f} = 1$. Thus, the magnetic field can be used to tune the linearity of the VI-characteristics and consequently, the linewidth.

2 Supplementary note 2: RSJ model

The resistively-shunted junction (RSJ) model allows to accurately describe single SNS Josephson junctions [1–3]. The model is schematically shown in Fig. 2a, where the junction can be modeled as a superconducting current channel governed by the Josephson equation

$$I_s = I_c \sin \phi, \tag{1}$$

with I_s the supercurrent, I_c the critical current and ϕ the phase difference – and a resistive quasiparticle channel with ohmic behavior

$$I_N = V_j / R_N, \tag{2}$$

with I_N the quasiparticle current, V_j the voltage over the junction and R_N the junction resistance, which can be approximated as the constant normal state resistance for SNS junctions. The total current I can be calculated using Kirchoff's current law

$$I = I_c \sin \phi + \frac{V_j}{R_N}. \tag{3}$$

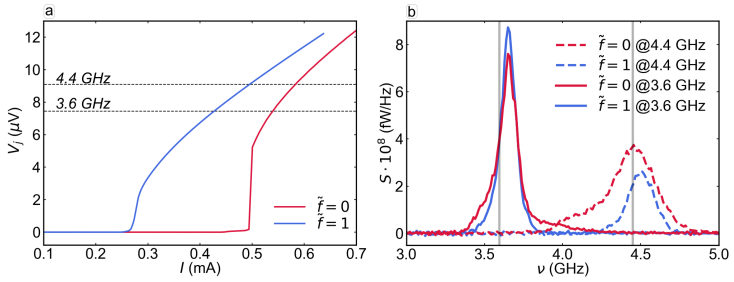

Fig. 1 Effect of non-linear VI characteristics on the emitted spectra. a VI curves at $\tilde{f} = 0$ and $\tilde{f} = 1$. **b** Measured spectra at 3.6 GHz and 4.4 GHz at $\tilde{f} = 0$ and $\tilde{f} = 1$. The grey lines represent the Josephson frequency V_j / Phi_0 for each peak.

Equation 3 can be rewritten in terms of the phase difference using the second Josephson equation ($V_j = \frac{\Phi_0}{2\pi}\frac{d\phi}{dt}$), leading to

$$I = I_c \sin\phi + \frac{1}{R_N}\frac{\Phi_0}{2\pi}\frac{d\phi}{dt}, \tag{4}$$

which can be rewritten as

$$\frac{d\phi}{dt} = \frac{2eI_cR_N}{\hbar}(i - \sin\phi), \tag{5}$$

with $i = I/I_c$ the reduced current. The time-dependent voltage $V_j(t)$ can be found by integrating equation 5 and using the second Josephson equation. The characteristic time of the junction is defined as:

$$\tau_c = \frac{\hbar}{2eR_NI_c}. \tag{6}$$

When a DC current bias is applied with $i < 1$, the current is purely carried by a supercurrent and the voltage is zero. As the bias current is increased to $i > 1$, the current can no longer flow as a pure supercurrent and some of it has to flow through the resistive channel. This results in an oscillating voltage as a function of time, of which simulations are shown in the inset of Fig. 2a. For low bias currents the $V_j(t)$ dependence is very anharmonic, while for higher bias currents it behaves almost like a perfect sine. The average voltage as function of applied current bias has the following relationship: $< V_j(t) >= I_cR_N\sqrt{i^2 - 1}$, shown in Fig. 2a.

3 Supplementary note 3: Theoretical emission power as function of applied voltage

Using the RSJ model, it is possible to simulate an emission map, shown in Fig.2b, from which the expected monotonic behavior of the emission power can already be seen. When biased with a DC current, the oscillating voltage contains harmonics, of which the amplitudes are given by [4, 5]

$$|V_n| = V_c\frac{2\bar{v}}{(\sqrt{1+\bar{v}^2}+\bar{v})^n}, \tag{7}$$

where $\bar{v} = \sqrt{i^2 - 1}$, with $i = I/I_c$ the reduced current, $V_c = I_cR_j$ is the critical voltage, and n the order of the harmonic. This relation is plotted in the inset of in Fig. 2b for the first and second harmonic as a function of the applied junction voltage in units of GHz, where experimentally determined values of $R_j = 0.33\ \Omega$ and $I_c = 495/14\ \mu$A $= 35\ \mu$A were used, resulting in a characteristic voltage of $V_c = 12\ \mu$V. The amplitude of the first harmonic of the voltage oscillation increases monotonically, while that of the second harmonic decreases after a voltage corresponding to 2 GHz. As the emission power is determined by the amplitude of the voltage oscillations, the available power

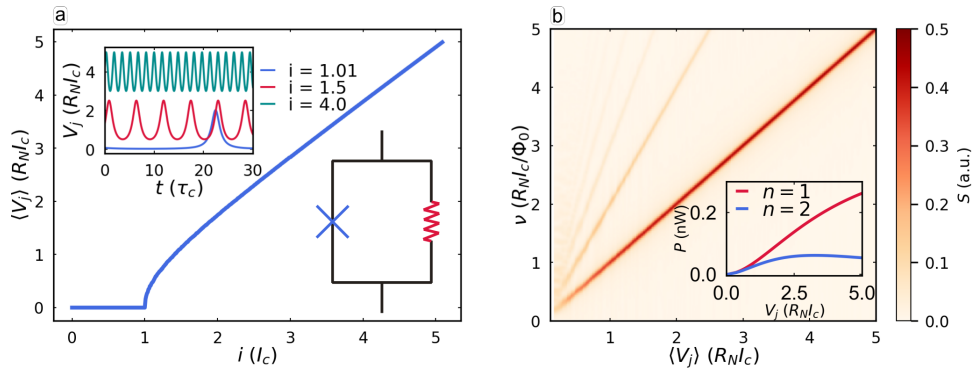

Fig. 2 Results of the RSJ simulations. a Simulated VI curve using the RSJ model. The lower inset shows the circuit representation of the RSJ model. The upper inset shows the simulated time dependence of the oscillating voltage. **b** Radiation map from simulated RSJ model. The inset shows the power determined by the voltage oscillations $|V_n|$ of the voltage oscillations for the first ($n = 1$) and second ($n = 2$) harmonic.

should have monotonical behavior as a function of applied voltage, which is in contrast to our experimental findings.

4 Supplementary note 4: Background signal as function of temperature

The thermal noise increases with temperature as can be seen in Fig. 3, which shows the measured background power density signal as a function of frequency for different temperatures when no bias is applied to MoGe-bot. The combination of increasing background power with increasing temperature and decreasing power of Josephson emission with decreasing critical current [according to Equation (7)] makes it difficult to measure radiation at 4.2 K.

5 Supplementary note 5: SEM image of MoGe-top and MoGe-bot

Fig. 4 shows a SEM image of MoGe-top and MoGe-bot. Fig. 4a shows the full structure, with both the top and bottom transport bridges in a single device. Fig. 4b and c show details of MoGe-top and MoGe-bot, respectively.

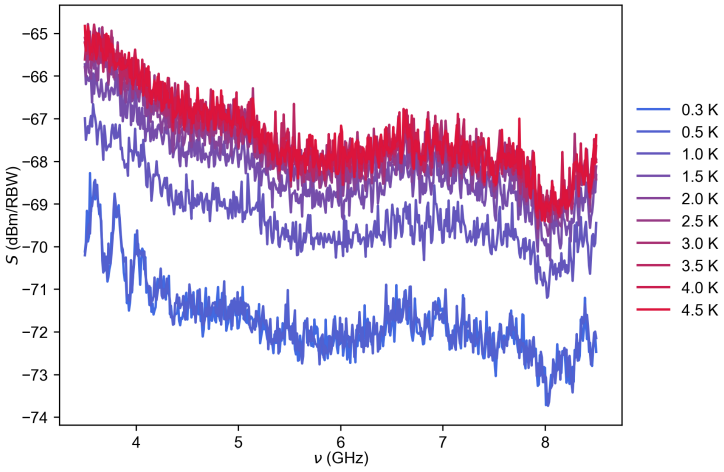

Fig. 3 Thermal background signal as function of frequency for temperatures between 300 mK and 4 K.

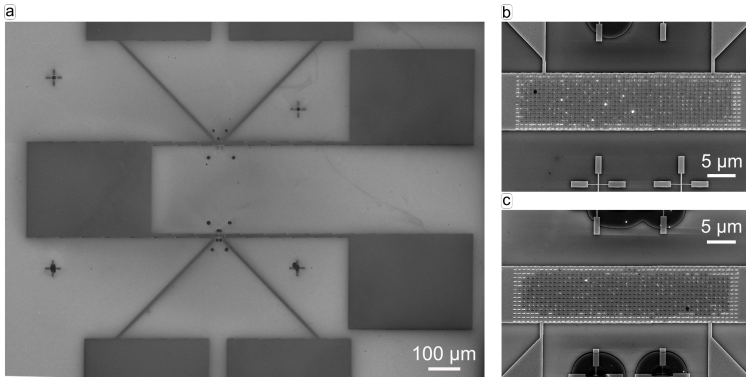

Fig. 4 **a** SEM image of Device 1. **b** and **c** are details of the JJ arrays of samples MoGe-top and MoGe-bot respectively.

References

[1] Panghotra, R. *et al.* Giant fractional Shapiro steps in anisotropic Josephson junction arrays. *Commun. Phys.* **3**, 1–8 (2020). URL https://www.nature.com/articles/s42005-020-0315-5. Publisher: Nature Publishing Group.

[2] Raes, B. *et al.* Fractional Shapiro steps in resistively shunted Josephson junctions as a fingerprint of a skewed current-phase relationship. *Phys. Rev. B* **102**, 054507 (2020). URL https://link.aps.org/doi/10.1103/PhysRevB.102.054507. Publisher: American Physical Society.

[3] Tinkham, M. *Introduction to Superconductivity* 2 edn (McGraw-Hill, New York, 1996).

[4] Jain, A., Likharev, K., Lukens, J. & Sauvageau, J. Mutual phase-locking in josephson junction arrays. *Phys. Rep.* **109**, 309–426 (1984). URL https://www.sciencedirect.com/science/article/pii/0370157384900024.

[5] Lukens, J. E., Jain, A. K. & Wan, K. L. Weinstock, H. & Nisenoff, M. (eds) *Application of josephson effect arrays for submillimeter sources.* (eds Weinstock, H. & Nisenoff, M.) *Superconducting Electronics*, 235–258 (Springer Berlin Heidelberg, Berlin, Heidelberg, 1989).